## Angle-dependent switching in a magnetic tunnel junction containing a synthetic antiferromagnet

Cite as: Appl. Phys. Lett. 120, 212401 (2022); https://doi.org/10.1063/5.0093044 Submitted: 25 March 2022 • Accepted: 09 May 2022 • Published Online: 23 May 2022

🔟 Hao Chen, Brad Parks, 🔟 Qiang Zhang, et al.







Lock-in Amplifiers up to 600 MHz



Zurich







# Angle-dependent switching in a magnetic tunnel junction containing a synthetic antiferromagnet

Cite as: Appl. Phys. Lett. **120**, 212401 (2022); doi: 10.1063/5.0093044 Submitted: 25 March 2022 · Accepted: 9 May 2022 · Published Online: 23 May 2022







Hao Chen, 1 D Brad Parks, 1,a) Qiang Zhang, 2,b) D Bin Fang, 2 Xixiang Zhang, 2 D and Sara A. Majetich 1,c)

#### **AFFILIATIONS**

- <sup>1</sup>Physics Department, Carnegie Mellon University, Pittsburgh, Pennsylvania 15213-3890, USA
- <sup>2</sup>Materials Science and Engineering Department, King Abdullah University of Science and Technology, Thuwal 23955-6900, Saudi Arabia
- a) Present address: Intel Ronler Acres, 2501 NEE Century Blvd., Hillsboro, OR 97124 USA. Electronic mail: bradley.parks@intel.com
- b) Present address: New York University Abu Dhabi, P. O. Box 129188, Abu Dhabi, United Arab Emirates. Electronic mail: qz19@nyu.edu
- c) Author to whom correspondence should be addressed: sara@cmu.edu

#### **ABSTRACT**

The angle dependence of field-induced switching was investigated in magnetic tunnel junctions with in-plane magnetization and a pinned synthetic antiferromagnet reference layer. The  $60 \times 90 \, \mathrm{nm}^2$  elliptical nanopillars had sharp single switches when the field was applied along the major axis of the ellipse, but even with small ( $20^\circ$ ) deviations, reversal occurred through an intermediate state. The results are interpreted with a model that includes the external applied field and the effective fields due to shape anisotropy and the fringe field of the synthetic antiferromagnet and used to extract the magnetization direction at various points in the magnetoresistance loop. The implications for faster spintronic probabilistic computing devices are discussed.

Published under an exclusive license by AIP Publishing. https://doi.org/10.1063/5.0093044

Stoner and Wohlfarth first investigated angle dependent switching of the magnetic moment in thermally stable ellipsoidal magnetic nanoparticles, leading to the famous astroid diagram of the coercivity as a function of the applied field magnitude and direction. The Stoner-Wohlfarth theory has since been extended to field-driven reversal in more complex cases, including combinations of cubic and uniaxial anisotropy and multi-jump magnetization reversal<sup>2</sup> and single nanoparticles.<sup>3–7\*</sup> While nominally a static phenomenon,<sup>8</sup> it has recently been extended to explain dynamics.<sup>9,10</sup> The model has been applied to magnetic recording media<sup>11,12</sup> and sensors.<sup>13</sup> It has also been invoked in spintronics for patterned thin films and magnetic nanopillars. 14-16 Spin currents have been used to bias thin film magnets in one direction, distorting the astroid, 14 and experiments with notched spin valve elements show that magnetization reversal is complex and may involve domain wall nucleation, pinning, and annihilation. 17-19 In this study, we examined angle-dependent reversal in small elliptical patterned magnetic tunnel junctions (MTJs) (60 × 90 nm<sup>2</sup>), which favor single domains and coherent rotation. The magnetization direction of an individual magnetic layer is detected through the tunnel magnetoresistance (TMR). We find that the astroid behavior is complicated by the presence of the fringe field from an underlying synthetic antiferromagnet (SAF), which distorts the angle and magnitude of the net effective field. The results are relevant not

only for field-induced switching but also in spintronics for probabilistic computing applications requiring low energy barriers—including random number generators, analog multiplication, invertible logic gates, and integer factorization. <sup>20–22</sup> Normally, the anisotropy or magnetic volume is adjusted to change the barrier for reversal in a nanomagnet. Our findings demonstrate that an additional parameter can be used if the nanomagnet is part of a tunnel junction with a synthetic antiferromagnet.

The magnetoresistance hysteresis loops for MTJ devices were measured while the external field was applied in the sample plane with various angles  $\theta=0^\circ$  between the applied field and the major axis of the ellipse (MAE). (Details about the sample preparation are included in the supplemental material, Sec. S1, and further information about the measurements is in Secs. S2–S4.) A schematic of the measurement is shown in Fig. 1(a). A series of hysteresis loops were recorded for different values of  $\theta$ . At  $0^\circ$  [Fig. 1(b)], there is a relatively square loop with a small coercivity (4 Oe), shifted to positive fields by 26 Oe. While the resistance is almost flat for negative fields following the sharp switch, at positive fields there is curvature prior to saturation, suggesting gradual rotation of the magnetic moment. When the applied field is at  $20^\circ$  [Fig. 1(c)], there is less rotation on the positive branch and also a small kink in the hysteretic region at  $\sim$ 35 Oe, shifting the upper part (shown in red) to slightly higher fields. At  $0^\circ$  and  $20^\circ$ , the

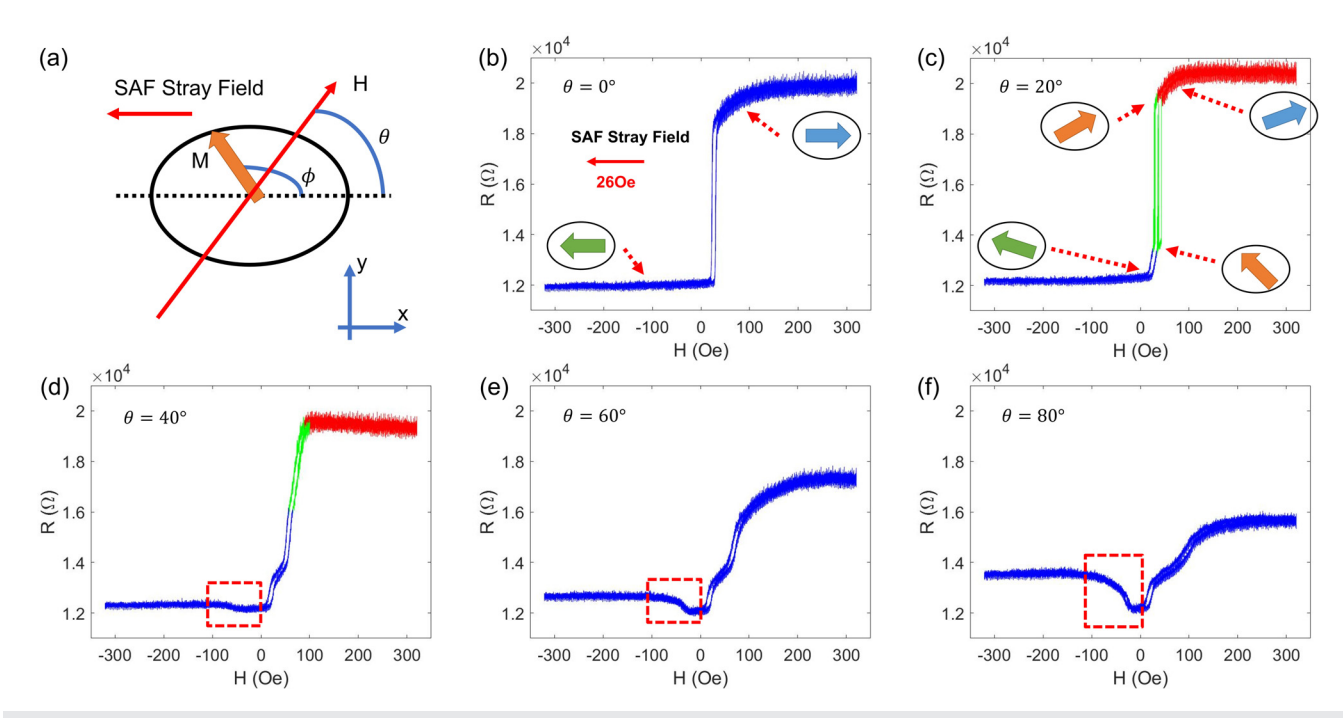


**FIG. 1.** Magnetoresistance hysteresis loops. (a) Schematic top view of the MTJ showing definitions of the angles  $\theta$  and  $\phi$ . Resistance as a function of the applied field for  $\theta = 0^{\circ}$  (b),  $20^{\circ}$  (c),  $40^{\circ}$  (c),  $40^{\circ}$  (d), and  $80^{\circ}$  (e). The colors of different sections of the hysteresis loops refer to different energy barrier schematics shown in Fig. 2, and the orange arrows show the magnetization directions at different points of the curves.

resistance values at  $\pm 300$  Oe are comparable, but by  $40^{\circ}$  they begin to change. For all angles, the zero-field resistance is the same and would always be the lowest resistance measured in the hysteresis loops. This is taken as the parallel resistance, R<sub>p</sub>. In Fig. 1(d), the resistance jumps to a slightly higher level at H = -60 Oe and then remains flat. On the positive side, the resistance decreases slightly, but gradually above +100 Oe as the magnetic field increases (shown in red). The upper hysteretic region (shown in green) has more of a tilt than that at 20° and is shifted toward higher fields. At 60° and 80° [Figs. 1(e) and 1(f), respectively], the trends continue. The -300 Oe resistance gets higher, and the +300 Oe resistance drops, making the antiparallel resistance region near H=0 appear more prominent. The width of the antiparallel resistance region narrows with increasing angle. The position of the low field hysteretic region near +30 Oe stays approximately constant, while the higher field hysteretic region skews more with increasing field, giving rise to more curvature in the top branch.

While there are some monotonic trends, some of the behavior is different from expectations for a Stoner–Wohlfarth astroid when rotating the direction of the applied field. The nanopillar here is a thin film ellipse rather than an ellipsoid and, in addition, has a stray field due to the synthetic antiferromagnet (SAF) below it. The SAF part of the MTJ consists of 2.5 nm of CoFe, with 0.85 nm of Ru and 2.5 nm of CoFeB on top, which is pinned by an 8 nm IrMn layer. We analyze the data in terms of three parameters: the shape anisotropy, the external magnetic field, and the SAF stray field. The shape anisotropy of the  $60 \times 90 \text{ nm}^2$  elliptical dot favors magnetization along the long axis. The SAF stray field is generated by two ferromagnetic components of the fixed layer. The direction of the SAF stray field could be calculated from the device TMR when H=0. At zero field, the device has a

TMR almost the same as  $R_p$  (12 k $\Omega$ ), representing a -x SAF stray field direction. The strength of the SAF field is then estimated to be  $\sim$ 26 Oe based on the field required to flip the free layer magnetization when the external field was applied along the MAE ( $\theta=0^{\circ}$ ) [Fig. 1(b)].

The relative angle between the free layer magnetization and the MAE,  $\phi$ , was calculated from the TMR using an empirical cosine relation

$$\phi = \cos^{-1}\left(\frac{R - \overline{R}}{(R_{ap} - R_P)/2}\right),\tag{1}$$

where R is the measured resistance,  $R_{ap}$  and  $R_p$  are the resistances when the free layer magnetization is anti-parallel and parallel to that of the reference layer, and  $\overline{R}=(R_{ap}+R_p)/2$ . For  $(\theta=0^\circ)$ , the  $+300\,\mathrm{Oe}$  resistance is assumed to be that of the antiparallel state,  $R_{ap}$ . The high field curvature in Fig. 1(b) may be due to a slightly rounded right end of the device introduced in the e-beam lithography process or alternatively to a small pinning effect. This makes a small range of angles accessible to the free layer magnetization other than along the MAE. The free layer magnetization will rotate first within this angle regime and then overcome the energy barrier and flip to the -x direction. The three components mentioned above are calculated in the form of their effective fields  $H_{eff}=E/\mu_0 MV$ , where E is the associated energy contribution,  $\mu_0$  is the vacuum permeability, M is the magnetization of CoFeB, and V is the magnetic volume

$$H = H_{\text{Anisotropy}} + H_{\text{Zeeman}} + H_{\text{SAF}}$$

$$= \left[ (8 \text{ Oe}) \sin^2 \phi + H_{\text{Offset}} \right] + \left[ -H_{\text{External}} \cos(\phi - \theta) \right]$$

$$+ \left[ (-26 \text{ Oe}) \cos(\phi - \pi) \right]. \tag{2}$$

The 4 Oe measured coercivity in Fig. 1(b) gives the lower bound of the shape anisotropy energy barrier, and the effective field of shape anisotropy is estimated by the hard axis component of the external field at an angle where the energy barrier is fully compensated. Given the experimental finding that a fully coherent rotation hysteresis loop was initially observed at an angle of  $\theta \sim 30^\circ$  (see supplementary material, Fig. S2), an 8 Oe shape anisotropy effective field is applied in the theoretical analysis.  $H_{\rm Offset}$  is a constant energy offset, which only depends on the shape of the device. <sup>23</sup> It is used as a reference energy level in the model and assumed to be zero in the later discussions.

The energy diagram is shown in Fig. 2(a) when the external field is applied along the MAE ( $\theta=0^{\circ}$ ), as in Fig. 1(b). As the external field is reduced from +320 to +46 Oe, the free layer magnetization stays in the  $\phi=0$  energy minimum (blue curve and arrow). When the external field decreases to 26 Oe and cancels the SAF stray field (orange curve and arrows), there are two energy minima. Here, the moment direction switches to  $\phi=\pi$ , consistent with the single sharp switch in the hysteresis loop of Fig. 1(b). Further reduction of  $H_{\rm external}$  lowers the single energy minimum (green curve and arrow).

When  $\theta=20^\circ$  [Fig. 1(c)], the free layer magnetic moment no longer jumps across the shape anisotropy energy barrier from  $\phi=0^\circ$  to  $\phi=180^\circ$  as the external magnetic field rotates toward the minor axis of the ellipse. The representative energies as a function of the magnetization angle  $\phi$  are shown in Fig. 2(b). A combination of coherent rotation and free layer switching is seen in the hysteresis loop. Starting from a high positive external field, the external field initially dominates, and the free layer is nearly pinned to the external field direction. Only one energy minimum exists in the energy diagram, shown as the blue line in Fig. 2(b). As the external field decreases, the SAF stray field becomes comparable in magnitude, and the free layer starts to rotate coherently from the external field direction, shown as the red top

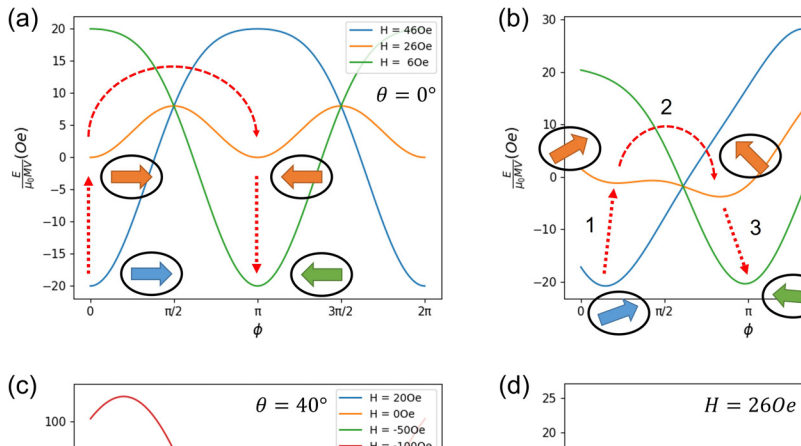
branch in Fig. 1(c) and arrow 1 in Fig. 2(b). An intermediate state with  $\phi=135^\circ$  was observed, representing a single energy minimum for the free layer magnetization as with a Stoner–Wohlfarth astroid. Assisted by the thermal fluctuations, the magnetization could jump between local energy minima following arrow 2 in Fig. 2(b) into the intermediate state. This magnetization jump is also observed as the green part of Fig. 1(c), and telegraphing between the two states occurs because the energy barrier height is comparable to thermal energy. As the external field is further reduced, after the switch, the energy minimum slowly relaxed from the intermediate state toward the -x direction following arrow 3 in Fig. 2(b).

While the resistance stays almost the same in the lower branch in Fig. 1(c), a curvature was observed at a field around -50 Oe when the external field is applied at higher angles, as shown by the red boxes in Figs. 1(d)–1(f). This results from coherent rotation of the magnetization from the SAF stray field direction (-x) toward the external field direction. When the external field is exactly zero, the magnetization would be pinned by the SAF stray field along the -x direction and  $R_p$  will be measured. As the negative field is turned on, the energy minimum gradually shifts toward the external field direction, and the transition happens at a field around -50 Oe. Figure 2(c) shows the energy diagrams for the described magnetization rotation when the external field is applied at  $\theta=40^\circ$ . The magnetization rotation is always monotonic as the field is decreasing or increasing but the resistance will drop first to  $R_p$  and then increase as the magnetization rotates past  $\phi=\pi$ .

Another way to view the data is to consider the net field components along the major and minor axes of the ellipse. At relatively small  $\theta$  angles, such as 20°, the minor axis component of the external field is not enough to compensate the energy barrier created by shape anisotropy, so a switch was observed, as shown in the green part of Fig. 1(c).

H = 460e H = 260e H = 60e

 $\theta = 20^{\circ}$ 



 $3\pi/2$ 

(d)  $_{25}$   $_{20}$   $_{15}$   $_{10}$   $_{15}$   $_{15}$   $_{10}$   $_{15}$ 

**FIG. 2.** Normalized energy barrier as a function of the magnetization direction  $\phi$  at different values of the magnetic field for the field along  $\theta=0^\circ$  (a),  $20^\circ$  (b), and  $40^\circ$  (c). (d) Normalized energy barrier vs  $\phi$  at H = 26 Oe as a function of angle, showing the gradual disappearance of a local maximum near  $\pi/2$ .

-50

-100

However, the minor axis component of the external field energy would be sufficient to compensate for the shape anisotropy energy at larger  $\theta$  angles [Fig. 1(d)]. The free layer magnetization rotates smoothly across the hard axis while staying in the energy minimum state. The explanation is similar for higher angles [Figs. 1(e) and 1(f)]; the only difference would be in the pinned position at the two ends of the hysteresis loop. The energy diagrams for the three considered angles at the field where the magnetization switch happens are shown in Fig. 2(d). The energy barrier between the states clearly exists when  $\theta=20^\circ$  and gradually disappears as the external field angle is increasing. If the SAF stray field is along the MAE ( $\theta=0^\circ$ ), then the measured resistances for  $\theta=90^\circ$  should be equal, provided the field is large enough.

The direction of the free layer magnetization  $\phi$  is plotted as a function of the external field angle  $\theta$  at the maximum (320 Oe) and minimum (-320 Oe) measured fields in Fig. 3. Here, a dashed line shows the expectations with a coherent rotation model if there were no additional SAF field. The SAF stray field pulls the free layer magnetization toward the -x direction, the direction of the SAF field, in all cases. The shape anisotropy can be ruled out since the measured curves do not have hard axis mirror symmetry. Though the external field here was up to ten times as strong as the SAF stray field, it was not enough to fully pin the free layer magnetization unless  $\theta$  was small. As the external field decreases, the SAF stray field gradually becomes the dominant factor in determining the free layer magnetization direction  $\phi$ . Detailed plots for the measured  $\phi$  in the fields of  $\pm 220$ ,  $\pm 120$ , and  $\pm 20$  Oe are shown in Fig. S3. For the larger fields, the qualitative trends are similar to those at  $\pm$  320 Oe. At  $\pm$  20 Oe, no states with  $\phi < 90^{\circ}$  are energetically favorable due to the SAF stray field.

The deviation between the free layer magnetization direction  $(\phi)$  and the external field direction  $(\theta)$  is plotted in Fig. 4 for different cases of the total energy. Angle  $\phi$  was determined by finding the energy minimum while the external field angle  $\theta$  varied between  $0^{\circ}$  and  $180^{\circ}$ . Starting from the case where only external field term is considered (green line), the free layer magnetization follows the external field

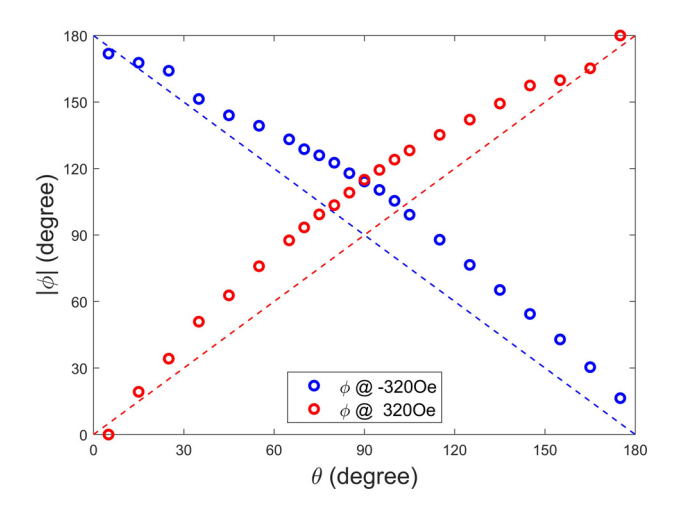


**FIG. 3.** Absolute value of the high field magnetization angle  $|\phi|$  as a function of the field angle  $\theta$ . Circles are taken from the experimental magnetoresistance hysteresis loops. Dashed lines are calculated for a coherent rotation model without the additional SAF field. The sign of  $\phi$  is determined by the sign of the y component of the external field. Figure S3 shows results for other fields.

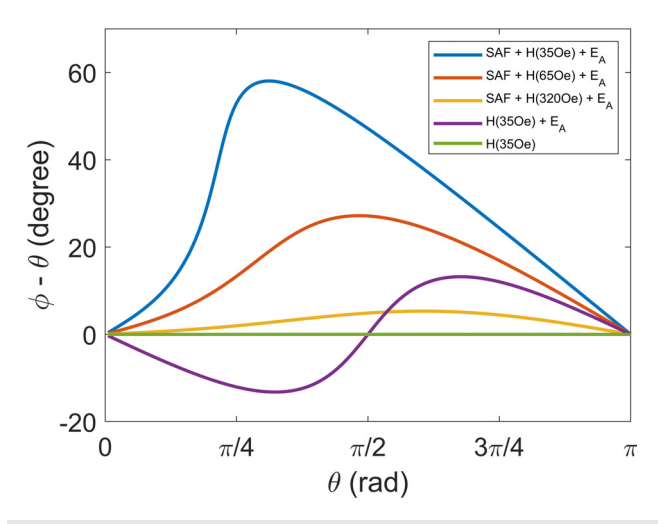


FIG. 4. Deviation between magnetization and applied field angles as a function of the applied field angle, dependent on the effective field terms. There is no deviation with just an external field of 35 Oe (green). Positive and negative differences appear with addition of the small anisotropy field (purple), but only positive deviations are seen when the larger SAF field is also included (blue). Increasing the magnitude of the external field increases the deviations and shifts the angle where the difference is largest (orange and yellow).

direction and the deviation is always zero. Adding the shape anisotropy (purple line) makes the free layer magnetization favor the MAE, which results in a positive deviation when  $\theta > 90^{\circ}$  and negative deviation when  $\theta < 90^{\circ}$ . The negative deviation is no longer observed once the SAF stray field is introduced (blue line), and the free layer magnetization will always be pulled toward the 180° direction. These positive deviations will be compressed as the external field is increased, but a  $6^{\circ}$  deviation is still observable even with a 320 Oe external field. This suggests that the SAF stray field is the main cause of the deviation observed in Fig. 3. The difference between the experimental observed deviation of up to  $20^{\circ}$  and the theoretically predicted  $\sim 6^{\circ}$  may be due to slight modification of the magnetization configuration of the SAF structure caused by the 320 Oe external field, which would affect the SAF stray field condition and change the fixed layer direction. Both these factors could give rise to the difference between the experimental value and theoretical prediction. The effect of varying the SAF stray field strength was also studied, and there was also a positive correlation between the size of the deviation and the magnitude of the SAF field. Results are shown in Fig. S4.

We have seen that the free layer moment saturates for fields of 300 Oe applied along the MAE directions ( $\theta=0^\circ,180^\circ$ ), but for other values of  $\theta$ , the SAF field causes distortions. Here, the SAF field at angle  $\pi$  led to magnetic moment angles  $\phi$  that were greater than expected from the external field direction. More significant are the deviations that occur at smaller applied fields. An energy barrier model including the effects of anisotropy, SAF, and external fields explains regions in the resistance hysteresis loops associated with gradual rotations as well as jumps to intermediate states where the moment is tilted, relative to the major axis of the ellipse. Telegraphing is observed only for a small angular range, and the two states involved do not have antiparallel magnetization directions. This is significant because it implies that very low energy barriers could be achieved without an

external field by adjusting the major axis of the MTJ ellipse relative to the stray field of the synthetic antiferromagnet.

The results presented here are based on magnetoresistance measurements on nanopillars as a function of the applied magnetic field but are also relevant for magnetic nanopillars driven by spin transfer torque or spin-orbit torque. Our results show the impact of misorientation of the external field, relative to the anisotropy and SAF fields. At current values required to switch a typical nanopillar (mA), the effective field can be on the order of 400 Oe.<sup>19</sup> The connection between a spin polarized current and effective field has also been made to explain current-driven domain wall motion<sup>24</sup> and spin Hall magnetoresistance in heavy metal-CoFeB bilayers.<sup>25</sup> While those systems are more complex, in patterned structures the combination of misoriented fringe fields with the effective spin torque fields could alter device performance. Our data show the importance of including all contributions in a single framework.

These findings have significant potential impact on the design of magnetic tunnel junctions for probabilistic computing,  $^{20-22}$  where low energy barriers  $\sim k_B T$  are desirable so that statistical averages can be obtained within a short time window. Most experimentally tested spintronic devices have used structures developed for high energy barrier applications (>40  $k_B T$ ). Our results suggest an alternative approach to reduce the energy barrier by intentional misalignment of the SAF field and effective anisotropy fields. By compensating for these fields, with some adjustment of the pattern shape, it is feasible to achieve zero-field telegraphing with a very low energy barrier. The two states would not have antiparallel magnetization, but the difference in resistance would still be on the order of  $k\Omega$ .

See the supplementary material for a detailed description of the nanofabrication, and additional results for magnetoresistance as a function of angle, deviation of the free layer magnetization direction at different field magnitudes, and the influence of the SAF field magnitude on the deviation.

S.A.M. would like to acknowledge financial support from the U.S. National Science Foundation under Grant No. ECCS-2004559. X.X.Z. would like to acknowledge the financial support by King Abdullah University of Science and Technology (KAUST), Office of

Sponsored Research (OSR) under Award No. CRF-2019-4081-CRG8.

### AUTHOR DECLARATIONS Conflict of Interest

The authors have no conflicts to disclose.

#### **DATA AVAILABILITY**

The data that support the findings of this study are available from the corresponding author upon reasonable request.

#### REFERENCES

- <sup>1</sup>E. C. Stoner and E. P. Wohlfarth, Philos. Trans. R. Soc. London, Ser. A 240, 599 (1948).
- <sup>2</sup>A. Thiaville, J. Magn. Magn. Mater. **182**, 5 (1998).
- <sup>3</sup>W. Wernsdorfer, E. B. Orozco, K. Hasselbach *et al.*, Phys. Rev. Lett. **78**, 1791 (1997).
- <sup>4</sup>E. Bonet, W. Wernsdorfer, B. Barbara et al., Phys. Rev. Lett. 83, 4188 (1999).
- <sup>5</sup>W. Wernsdorfer, C. Thirion, N. Demoncy *et al.*, J. Magn. Magn. Mater. **242**, 132 (2002).
- <sup>6</sup>C. Thirion, W. Wernsdorfer, and D. Mailly, Nat. Mater. 2, 524 (2003).
- <sup>7</sup>M. Lederman, G. A. Gibson, and S. Schultz, J. Appl. Phys. 73, 6961 (1993).
- <sup>8</sup>C. Tannous and J. Gieraltowski, Phys. B 403, 3563 (2008).
- <sup>9</sup>G. Amanoloaei, A. Stancu, and L. Stoleriu, IEEE Magn. Lett. **12**, 610305 (2021).
- 10 J. L. F. Cuñado, A. Bollero, T. Perez-Castaneda et al., Sci. Rep. 7, 13474 (2017).
- <sup>11</sup>B. Valcu, T. McDaniel, and X. Wang, IEEE Trans. Magn. **45**, 3565 (2009).
- <sup>12</sup>R. Wood, IEEE Trans. Magn. **45**, 100 (2009).
- <sup>13</sup>F. Bruckner, B. Bergmair, H. Brueckl *et al.*, J. Magn. Magn. Mater. **381**, 344 (2015).
- <sup>14</sup>Y. Henry, S. Mangin, J. Cucchiara et al., Phys. Rev. B **79**, 214422 (2009).
- 15 S. Yan, Z. Sun, and Y. B. Bazaliy, Phys. Rev. B 88, 054408 (2013).
- <sup>16</sup>N. Perrissin, N. Cacoilo, G. Gregoire et al., J. Phys. D: Appl. Phys. 52, 505005 (2019).
- <sup>17</sup>D. B. Gopman, D. Bedau, S. Mangin et al., J. Appl. Phys. **115**, 113910 (2014).
- <sup>18</sup>D. B. Gopman, D. Bedau, S. Mangin et al., Appl. Phys. Lett. **100**, 062404 (2012).
- Cucchiara, S. Le Gall, E. E. Fullerton et al., Phys. Rev. B 86, 214420 (2012).
   D. Vodenicarevic, N. Locatelli, A. Mizrahi et al., Phys. Rev. Appl. 8, 054045 (2017).
- <sup>21</sup>W. A. Borders, A. Z. Pervaiz, S. Fukami *et al.*, Nature **573**, 390 (2019).
- <sup>22</sup>M. Bapna and S. A. Majetich, Appl. Phys. Lett. 111, 243107 (2017).
- <sup>23</sup>H. Chang and J. Burns, J. Appl. Phys. 37, 3240 (1966).
- <sup>24</sup>S. Emori, E. Martinez, K.-J. Lee et al., Phys. Rev. B **90**, 184427 (2014).
- <sup>25</sup>A. Magni, V. Basso, A. Sola *et al.*, IEEE Trans. Magn. **58**, 4400205 (2022).